





RESEARCH PAPER

OPEN ACCESS 

## Auxiliary domains of the HrpB bacterial DExH-box helicase shape its RNA preferences

Stéphane Hausmann<sup>a</sup>, Johan Geiser <sup>a</sup>, Oscar Vadas <sup>a,b</sup>, Verena Ducret<sup>c</sup>, Karl Perron<sup>c</sup>, and Martina Valentini <sup>a</sup>

<sup>a</sup>Department of Microbiology and Molecular Medicine, CMU, Faculty of Medicine, University of Geneva, Geneva, Switzerland; <sup>b</sup>Protein Production Platform, Faculty of Medicine, University of Geneva, Geneva, Switzerland; <sup>c</sup>Microbiology Unit, Department of Botany and Plant Biology, University of Geneva, Geneva, Switzerland

### ABSTRACT

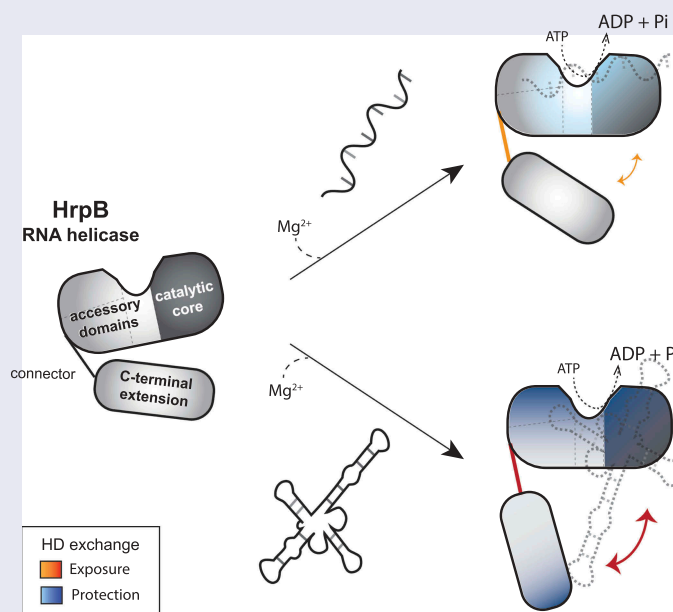
RNA helicases are fundamental players in RNA metabolism: they remodel RNA secondary structures and arrange ribonucleoprotein complexes. While DExH-box RNA helicases function in ribosome biogenesis and splicing in eukaryotes, information is scarce about bacterial homologs. HrpB is the only bacterial DExH-box protein whose structure is solved. Besides the catalytic core, HrpB possesses three accessory domains, conserved in all DExH-box helicases, plus a unique C-terminal extension (CTE). The function of these auxiliary domains remains unknown. Here, we characterize genetically and biochemically *Pseudomonas aeruginosa* HrpB homolog. We reveal that the auxiliary domains shape HrpB RNA preferences, affecting RNA species recognition and catalytic activity. We show that, among several types of RNAs, the single-stranded poly(A) and the highly structured MS2 RNA strongly stimulate HrpB ATPase activity. In addition, deleting the CTE affects only stimulation by structured RNAs like MS2 and rRNAs, while deletion of accessory domains results in gain of poly(U)-dependent activity. Finally, using hydrogen-deuterium exchange, we dissect the molecular details of HrpB interaction with poly(A) and MS2 RNAs. The catalytic core interacts with both RNAs, triggering a conformational change that reorients HrpB. Regions within the accessory domains and CTE are, instead, specifically responsive to MS2. Altogether, we demonstrate that in bacteria, like in eukaryotes, DExH-box helicase auxiliary domains are indispensable for RNA handling.

### ARTICLE HISTORY

Received 20 December 2019  
Revised 15 January 2020  
Accepted 18 January 2020

### KEYWORDS



RNA helicase; DExH-box; ATPase; HDX-MS; RNA-binding proteins; *Pseudomonas aeruginosa*




### Introduction

RNA molecules exert a wide multiplicity of functions in the cell beside protein synthesis, from regulation of gene expression to

DNA replication, maintenance of genome integrity, and others. Instrumental to the accomplishment of these cellular functions is the RNA folding, the abundance, and/or the interaction with RNA-binding proteins (RBPs) within ribonucleic-protein

**CONTACT** Martina Valentini  [Martina.Valentini@unige.ch](mailto:Martina.Valentini@unige.ch)  Department of Microbiology and Molecular Medicine, CMU, Faculty of Medicine, University of Geneva, Geneva, Switzerland

 Supplementary Data for this article can be accessed [here](#).

© 2020 The Author(s). Published by Informa UK Limited, trading as Taylor & Francis Group.  
This is an Open Access article distributed under the terms of the Creative Commons Attribution-NonCommercial-NoDerivatives License (<http://creativecommons.org/licenses/by-nc-nd/4.0/>), which permits non-commercial re-use, distribution, and reproduction in any medium, provided the original work is properly cited, and is not altered, transformed, or built upon in any way.

complexes (RNPs). It is thus not surprising that multiple proteins contribute to RNA metabolism and among them, a crucial role is performed by RNA helicases.

RNA helicases are enzymes that use the energy derived from the hydrolysis of nucleoside triphosphates (NTPs) to alter RNA structure, modify intermolecular interactions between RNAs and RBPs or modulate numerous structural transitions within RNPs [1]. Therefore, although unwinding of RNA duplex became their eponymous activity, the means by which RNA helicases act are much more diversified and can extend to RNA annealing, RNA clumping, or RBP displacement [2].

RNA helicases are found ubiquitously in all kingdoms of life and together with DNA helicases, are classified into six superfamilies according to conserved sequence motifs and shared structural elements [3]. The most conserved part of RNA helicases is their catalytic core, which is formed by two RecA-like domains containing up to 12 conserved sequence motifs involved in NTP hydrolysis, RNA binding, and unwinding/translocation [3,4]. The superfamily 2 comprises most of the RNA helicases and includes two large groups, DEAD-box, and DExH-box helicases, referring to one of the conserved motifs in the ‘catalytic core’ of the enzymes, i.e. motif II (Asp-Glu-Ala-Asp or Asp-Glu-variable-His, respectively) [3–5]. In addition to the core part, almost all RNA helicases possess one or more accessory domains at their N- and/or C-termini [3]. These domains appear to regulate enzyme activity by coordinating RNA binding, modulating protein NTPase activity, and/or providing a platform for interaction with protein partners [5]. Overall, the length, structure, and conservation of the accessory domain(s) are highly variable, making their mode of action hard to predict from their sequence [4].

All the DExH-box RNA helicases that have been structurally characterized to date share three accessory domains: a winged-helix (WH) domain, a helical bundle (HB) domain, and an oligonucleotide/oligosaccharide (OB) domain. In some instances, unique C-terminal and/or N-terminal extension(s) can be present in addition to the catalytic core and accessory domains [6–17]. The role of these auxiliary domains has been thoroughly investigated in many eukaryotic DExH-box proteins, while for prokaryotic ones the question remains unresolved [5,13]. In *Saccharomyces cerevisiae* (Sc) and *Chaetomium thermophilum* (Ct), for example, the accessory domains of Prp43 act as regulatory domains for RNA binding, participate together with the RecA2 domain in coupling ATP hydrolysis to RNA unwinding, and are indispensable for interaction with G-patch-containing proteins [7]. Another example is the OB-fold of the *Drosophila melanogaster* MLE helicase, which contributes to MLE RNA specificity by forming sequence-specific RNA interactions [6].

The first crystal structure of a bacterial DExH-box protein has been solved recently, namely the HrpB protein from *E. coli* [18,19]. HrpB structure revealed the presence of WH, HB, and OB accessory domains resembling the eukaryotic DExH-box accessory domains and a HrpB-unique C-terminal extension (CTE) [18,19]. HrpB thus provides the opportunity to investigate on the evolution of DExH-box proteins, particularly on what might be the ancestral role of the accessory domains, assessing conserved features across life domains and subsequent

acquisition of functions. In this study, we investigated the HrpB homolog from the bacterial opportunistic pathogen *Pseudomonas aeruginosa*. We performed an *in vivo* analysis of the phenotype of the *hrpB* mutant and we characterized *in vitro* the biochemical properties of HrpB, with a focus on the function of accessory domains. Combining enzymatic assays with hydrogen-deuterium exchange mass spectrometry (HDX-MS) data and mutational studies, we define here a role for HrpB accessory domains and CTE in RNA recognition and discrimination.

## Results

### Identification of the DExH-box protein HrpB in *P. aeruginosa* PAO1 and its domain conservation

HrpB-like proteins are found mainly in Proteobacteria and Actinobacteria, with few Firmicutes and Bacteroidetes showing *hrpB* acquisition probably by horizontal gene transfer [20]. In the *P. aeruginosa* PAO1 genome, the gene PA3961 encodes a predicted DExH-box helicase annotated as *hrpB* [21]. *P. aeruginosa* PAO1 HrpB (*PaHrpB*) has 47% amino acid sequence identity with *E. coli* HrpB (*EcHrpB*). By sequence alignment, we identified in *PaHrpB* the seven domains present in *EcHrpB*: the two RecA-like domains (RecA1 and RecA2), the accessory domains WH, HB, and OB domains, as well as a CTE (C-terminal extension) formed by a connector element (CON) and a C-terminal region (C-ter) (Fig. 1). The RecA-like core comprises the eleven helicase motifs and it constitutes the most conserved region not only among bacterial HrpB-like proteins (Supplementary Figure S1) but as well in eukaryotic DExH-box proteins (Supplementary Figure S2). Interestingly, sequence alignment of ~700 bacterial HrpB homologs revealed a ~70 amino acid-stretch in the C-terminal domain of HrpB (residues 754–825) that also displays a high degree of conservation, probably indicating an important role of these residues for the protein function (Supplementary Figure S1).

### Phenotypic characterization of the *P. aeruginosa* HrpB mutant

The phenotype of an *hrpB* mutant has been investigated in two bacterial species. An *hrpB* mutant of *Xanthomonas citri* exhibits an increased sliding motility, reduction in biofilm formation, and decreased virulence and survival on host leaves [22]. On the other hand, an *E. coli* *hrpB* mutant does not display a different phenotype compared to the wild-type in respect to motility, biofilm formation, response to heat, cold, osmotic, and oxidative stresses [18]. To investigate the function of HrpB in *P. aeruginosa*, we constructed an in-frame *hrpB* deletion and compared its phenotype to the wild-type. We analysed growth of the strains at different temperatures, as well as tolerance to H<sub>2</sub>O<sub>2</sub> or NaCl (to mimic oxidative or osmotic stress, respectively), motility (swimming, swarming, and twitching), biofilm formation, and virulence (using *Galleria mellonella* as model organism); however, no differences could be observed (Fig. 2). Since several bacterial RNA helicases play a role in cold adaptation [20], the phenotypic tests were also conducted at temperatures colder than 37°C (30°C and 16°C) but similar results were obtained (data

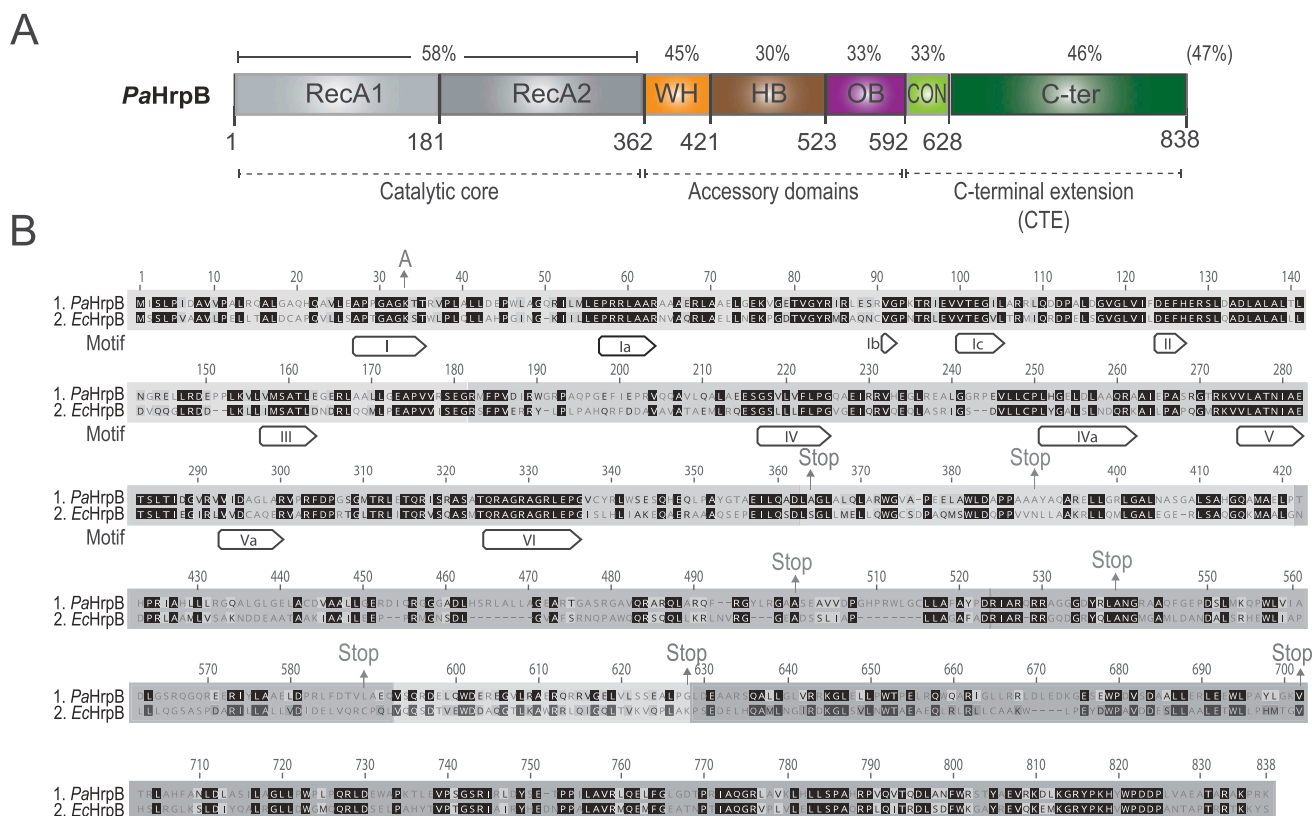


**Figure 1. *P. aeruginosa* HrpB domain organization.** (A) Linear representation of *P. aeruginosa* HrpB (PA3961), with the RecA1 and RecA2 domains in grey (light and dark grey, respectively), the winged-helix (WH) domain in orange, the helical bundle (HB) domain in brown, the oligonucleotide/oligosaccharide-binding (OB) domain in purple, the connector (CON) in light green, and the HrpB C-terminal (C-ter) region in dark grey. % indicate sequence identity with *E. coli* HrpB (NP\_414690.4). (B) Sequence alignment of *P. aeruginosa* (Pa<sub>1</sub>) and *E. coli* (Ec<sub>1</sub>) HrpB. Sequence region corresponding to the RecA-like, WH, HB, OB, CON, and C-ter domains are highlighted by boxes coloured as in A. Motifs I–VI are indicated while A and Stop indicate recombinantly produced HrpB variants (K33A or truncations, respectively).

not shown). Altogether, our results indicate that *P. aeruginosa* HrpB, like in *E. coli*, does not seem to perform the same role as in *X. citri*. In order to gain more insights into HrpB, we therefore applied a biochemical approach, with the aim of characterizing HrpB catalytic activity and its regulation.

### Characterization of the HrpB NTPase activity

The 838-amino acid PaHrpB protein was produced and purified in *E. coli* as N-terminal His<sub>10</sub>Smt3-tagged fusion (Fig. 3A). In parallel, we also purified a mutated version of His<sub>10</sub>Smt3-HrpB in which Lys33 of motif I (Walker A motif <sup>27</sup>APPGAGKT<sup>34</sup>), involved in ATP binding and hydrolysis [23], was replaced by alanine. His<sub>10</sub>Smt3-HrpB (referred to as HrpB herein) catalyzes the release of Pi from [ $\gamma$ -<sup>32</sup>P] ATP in the presence of poly(A) RNA and we found that the extent of ATP hydrolysis is proportional to enzyme concentration, the substrate being hydrolysed completely at saturating enzyme concentration (Fig. 3B). A specific activity of 0.052 nmol of ATP hydrolysed per ng of protein in 15 min is calculated from the slope of the titration curve in the linear range (this value translates into a turnover number of 371 min<sup>-1</sup>). A basal ATPase activity is observed even in the absence of poly(A), with 0.0051 nmol of ATP hydrolysed per ng of protein in 15 min (this value translates into a turnover of 36 min<sup>-1</sup>). Treatment with RNase A reduced about 2-fold the basal activity in the absence of poly(A) (data not shown), indicating that some RNA molecules co-purified with HrpB. As expected, the ATPase activity of the

HrpB<sub>K33A</sub> mutant, both in the presence and in the absence of poly(A), is less than 1% of the activity of wild-type enzyme stimulated by poly(A) (Fig. 3B). Overall, we estimate that poly(A) stimulates at least 10-fold ATP hydrolysis by HrpB. Of note, cleaving the N-terminal His<sub>10</sub>Smt3- tag does not affect the enzymatic activity (Supplementary Figure S3A, C and D).

The Q motif is a conserved element of DEAD-box helicases, upstream of motif I, that regulates ATP binding and hydrolysis as well as the RNA affinity and helicase activity [24]. It has been postulated that the absence of the Q motif in DEAH-box proteins allows them to non-specifically hydrolyse any NTPs. We assessed HrpB NTP substrate specificity by measuring colorimetrically the release of inorganic phosphate from NTPs and dNTPs. The extents of phosphate release by HrpB in the presence of poly(A) with CTP, GTP, and UTP substrates were 175%, 40%, and 170%, respectively, of the activity with the ATP substrate (Fig. 3C). The same trend is observed with dNTPs (Supplementary Figure S4). Noteworthy, the CTPase activity of EcHrpB was found 14-fold higher than the ATPase [18], while we found that PaHrpB hydrolyses pyrimidine only slightly better than purine (1.8-fold difference).

### Optimization of HrpB ATPase condition and kinetic parameters determination

The optimal reaction conditions for HrpB ATP hydrolysis were defined via systematic variations of the magnesium

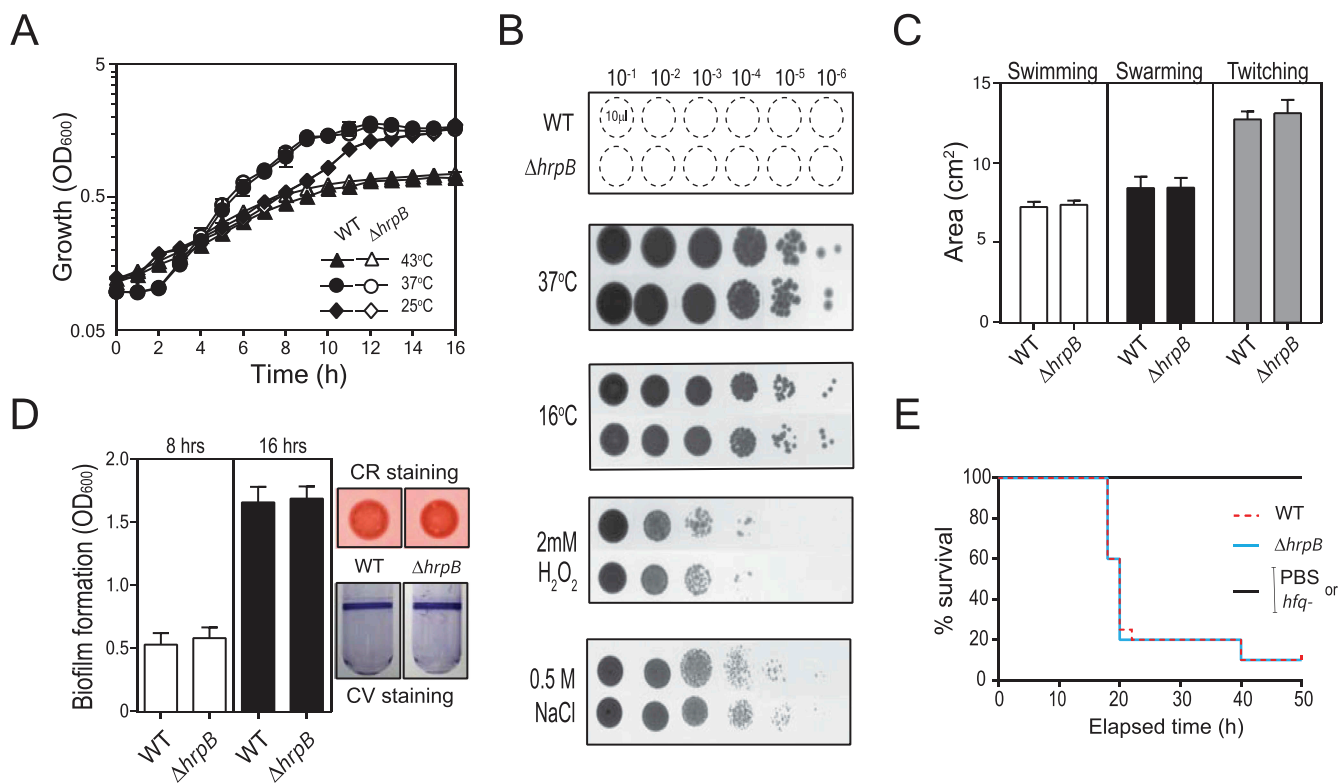


**Figure 2. Phenotypic characterization of *hrpB* mutant in *P. aeruginosa* PAO1.** (A) Growth properties of wild-type PAO1 (solid symbols) and  $\Delta hrpB$  mutant (empty symbols) in LB medium at 43°C (triangles), 37°C (circles) and 25°C (diamonds). (B) Survival assays of wild-type PAO1 and  $\Delta hrpB$  mutant to cold shock (16°C), oxidative stress (2 mM H<sub>2</sub>O<sub>2</sub>) and osmotic stress (0.5 M NaCl) as compared to 37°C growth. (C) Surface area covered by the swimming, swarming, and twitching cells ( $\pm$  standard deviation) of wild-type PAO1 or  $\Delta hrpB$  mutant as calculated by averaging data from four individual plates. (D) Biofilm formation of wild-type PAO1 or  $\Delta hrpB$  mutant measured by crystal violet staining or by Congo-red staining. (E) Survival curves of *G. mellonella* larvae infected with wild-type PAO1,  $\Delta hrpB$  or *hfq*-mutant. PBS, larvae injected with sterile physiological solution. Each experiment (A–D) was repeated at least with three different independent cultures for each strain, values indicated average from biological replicates  $\pm$  standard deviation. For experimental details see Material and Methods.

cofactor concentration, pH and salt. The concentration of magnesium in which we observe maximum Pi release, measured at non-saturating level of HrpB, was calculated to be between 300 and 600  $\mu$ M (Supplementary Figure S5A). Release of phosphate from nucleotide triphosphate by various superfamily 1 and 2 helicases is thought to require magnesium [4,25]. Surprisingly, we noticed that omitting magnesium in the ATPase reaction mixture reduced ATP hydrolysis by only 1.4-fold compared to the maximal activity. In addition, the ATPase activity was still observed without adding magnesium with HrpB purified by size-exclusion chromatography in a buffer containing 1 mM EDTA (Supplementary Figure S3D). Therefore, we performed an EDTA titration and we found that HrpB activity in the presence poly(A) was inhibited in a concentration-dependent manner by EDTA (Supplementary Figure S5B). We estimate from the EDTA titration curve an apparent IC<sub>50</sub> for EDTA of 125  $\mu$ M. The level of activity at 1 mM EDTA was 11% of the activity in the absence of EDTA and addition of magnesium or manganese in the reaction was restoring entirely HrpB activity (Fig. 3D). Overall, these results suggest that HrpB binds the metal avidly and it is reasonable to assume that the protein co-purifies with a magnesium ion bound to the catalytic core.

The HrpB ATPase activity was optimal at a range of pH 7.5–9.0 in Tris-HCl buffer, while it declined to 38% at pH 5.5 (Tris acetate) and was null at pH 4.0 (Supplementary Figure

S5C). Salt inhibited the HrpB ATPase activity, which was completely abolished at 250 mM of either NaCl or KCl (Supplementary Figure S5D). The apparent IC<sub>50</sub> values for NaCl and KCl were calculated at 50 and 60 mM, respectively, showing that increased ionic strength exerted a strong inhibitory effect on HrpB activity.

The kinetic parameters for HrpB were then determined by measuring the extent of Pi release during a 15-min reaction as a function of input [ $\gamma$ -<sup>32</sup>P] ATP concentration in the range of 3–250  $\mu$ M (Fig. 3E). A double-reciprocal plot of the data fits well to a linear function (Fig. 3E, inset). We calculated a K<sub>m</sub> of 20  $\pm$  4  $\mu$ M ATP and a k<sub>cat</sub> of 349  $\pm$  24 min<sup>-1</sup>. When compared to the values reported for the poly(A) dependent activity of the yeast DEXH-box helicases Prp43 and Prp22 (1700 min<sup>-1</sup> and 460 min<sup>-1</sup>, respectively), the turnover number of HrpB is similar to Prp22. The K<sub>m</sub> of HrpB for ATP in the presence of poly(A) is higher than the value reported for Prp43 (1.9  $\mu$ M) but lower as that noted for Prp22 (140  $\mu$ M) [26,27].

#### Quaternary structure of HrpB

We analysed the native size of HrpB by sedimentation of the protein through a 15 – 30% glycerol gradient. Marker proteins were included as internal standards. After centrifugation, the gradient fractions were analysed by SDS-PAGE (Supplementary Figure S6A). HrpB (107-kDa His<sub>10</sub>Smt3-polypeptide) sedimented

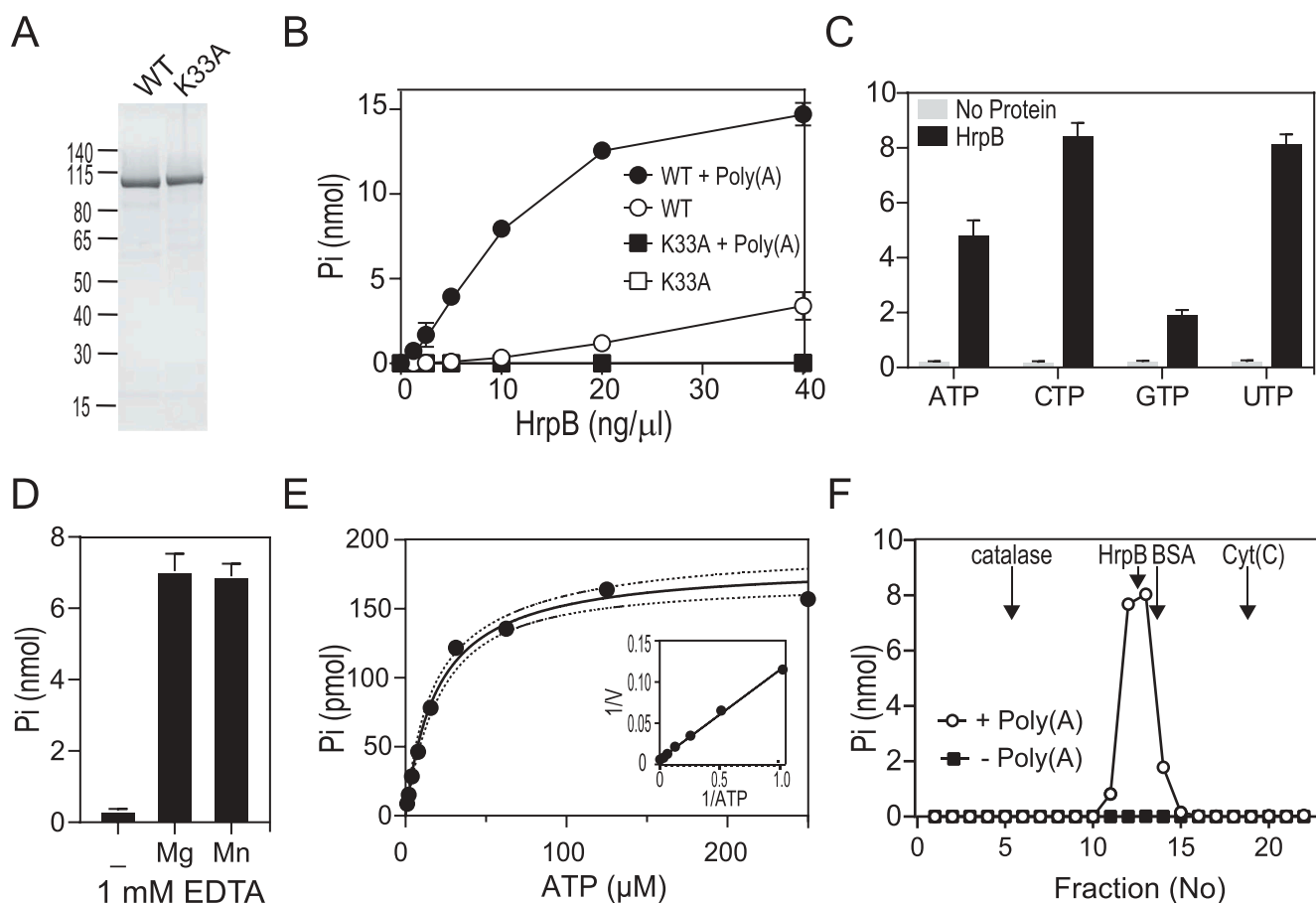


**Figure 3. ATPase activity of recombinant HrpB.** (A) HrpB purification. Aliquots (2.5  $\mu\text{g}$ ) of the nickel-agarose preparations of wild-type (WT) HrpB (lane 1), and mutant K33A (lane 2) were analysed by SDS-PAGE. The polypeptides were visualized by staining with Coomassie Blue dye. The positions and sizes (kDa) of marker polypeptides are indicated on the left. (B) ATPase. Reaction mixtures (15  $\mu\text{l}$ ) containing 50 mM Tris-HCl (pH 8.0), 1 mM DTT, 2 mM  $\text{MgCl}_2$ , 1 mM  $[\gamma\text{-}^{32}\text{P}]$  ATP, 250 ng/ $\mu\text{l}$  Poly(A) (or no RNA), and wild-type (WT) or K33A mutant as specified were incubated for 15 min at 37°C. Pi release was determined as described in Materials and Methods and was plotted as a function of input protein. (C) Nucleotide specificity. Reaction mixtures (15  $\mu\text{l}$ ) containing 50 mM Tris-HCl (pH 8.0), 1 mM DTT, 2 mM  $\text{MgCl}_2$ , 250 ng/ $\mu\text{l}$  Poly(A), 5 ng/ $\mu\text{l}$  WT HrpB (or no added enzyme) and 1 mM nucleotide triphosphate as specified were incubated for 15 min at 37°C. The reactions were quenched by adding 1 ml of malachite green reagent. Phosphate release was determined by measuring A620 and extrapolating the value to a phosphate standard curve. (D) Metal dependence. Reaction mixtures (15  $\mu\text{l}$ ) containing 50 mM Tris-HCl (pH 8.0), 1 mM EDTA, 1 mM DTT, 1 mM  $[\gamma\text{-}^{32}\text{P}]$  ATP, 250 ng/ $\mu\text{l}$  Poly(A), 5 ng/ $\mu\text{l}$  WT HrpB, and either No divalent cation (-) or 2 mM of the divalent chloride salt were incubated for 15 min at 37°C. The extends of ATP hydrolysis are plotted. (E) Kinetics parameter. Reaction mixtures (15  $\mu\text{l}$ ) containing 50 mM Tris-HCl (pH 8.0), 1 mM DTT, 250 ng/ $\mu\text{l}$  Poly(A), 5 ng/ $\mu\text{l}$  WT HrpB, and  $[\gamma\text{-}^{32}\text{P}]$  ATP as specified were incubated for 15 min at 37°C. The extent of Pi release is plotted as a function of ATP concentration. The inset shows a double-reciprocal plot of the rate of Pi formation. (F) ATPase activity profile of the glycerol gradient sedimentation of HrpB. Reaction mixtures (15  $\mu\text{l}$ ) containing 50 mM Tris-HCl (pH 8.0), 1 mM DTT, 2 mM  $\text{MgCl}_2$ , 1 mM  $[\gamma\text{-}^{32}\text{P}]$  ATP, 250 ng/ $\mu\text{l}$  Poly(A) (or no RNA), and 2  $\mu\text{l}$  of the indicated glycerol gradient fractions (Supplementary Figure S6) were incubated for 15 min at 37°C. The peaks of marker proteins are indicated by vertical arrows (Supplementary Figure S6). (B-D) Data are the average  $\pm$  SEMs from three independent experiments.

as a discrete peak (fraction 13), one fraction heavier than BSA (66 kDa). The ATPase activity profile in the presence of poly(A) paralleled the abundance of the HrpB polypeptide (Fig. 3F). A plot of the S values of the three standards versus fraction number yielded a straight line and we calculated an S value of 5.16 for His<sub>10</sub>Smt3-HrpB (Supplementary Figure S6B). We conclude from these results that HrpB is a monomer in solution with an elongated shape, which is consistent with the solved *Ec*HrpB structure [18,19]. Moreover, size-exclusion chromatography on a Superdex-200 column also shows that untagged HrpB elutes as a monomer (Supplementary Figure S3B).

### The HrpB ATPase activity displays RNA preferences

RNA helicases can differ in the degree of specificity or preference for RNA by various RNA recognition mechanisms [3]. The ATPase activity of *Ec*HrpB in the presence of a 26-mer single-

stranded RNA was shown to be 11 min<sup>-1</sup> [18], while we calculated a value 30-time higher (349 min<sup>-1</sup>) for *Pa*HrpB when using poly(A). This prompted us to investigate whether HrpB can differentiate among different RNA molecules as cofactors.

To probe the polyribonucleotide specificity of HrpB, we used poly(C), poly(G), and poly(U) in the ATPase reaction mixtures at equal concentrations. The titration profiles of the ATPase reaction of HrpB with poly(C), poly(G) and poly(U) substrates were 116%, 13%, and 19% of the activity with poly(A) substrate, respectively (Fig. 4A). We next tested smaller RNA molecules by using a 41-mer single-stranded RNA (R41) and we found that, although R41 was a good activator, the stimulation was 48% when compared to poly(A). In addition, a 41-mer DNA oligonucleotide (D41) of the same length and sequence of R41 (except T->U) was not able to stimulate the ATPase activity of HrpB when compared to the control without RNA (Fig. 4). This result implies that HrpB ATPase

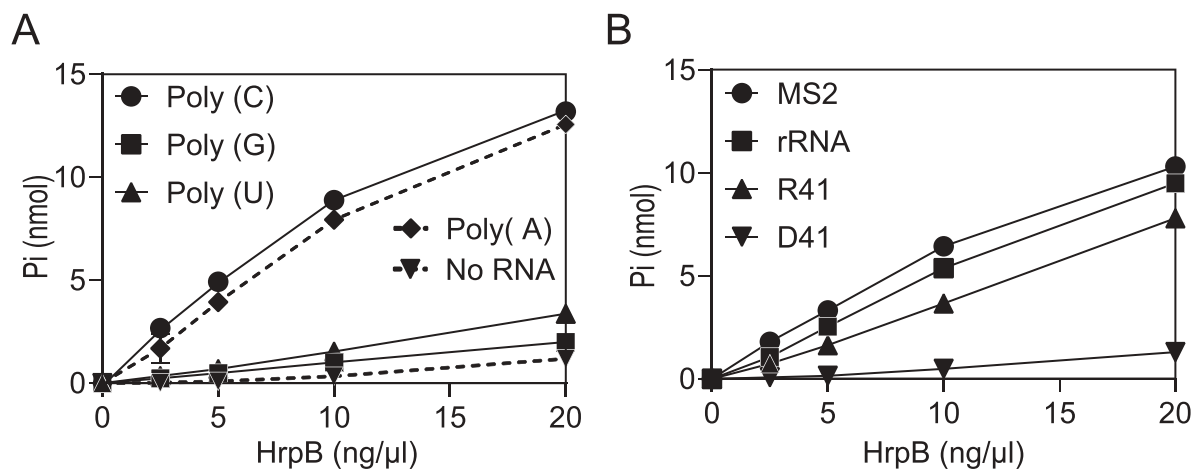


**Figure 4. HrpB nucleic acid cofactor dependence.** (A) Polyribonucleotide specificity. Reaction mixtures (15  $\mu$ l) containing 50 mM Tris-HCl (pH 8.0), 1 mM DTT, 2 mM MgCl<sub>2</sub>, 1 mM [ $\gamma$ -<sup>32</sup>P] ATP, 250 ng/ $\mu$ l of the indicated polyribonucleotide (or No RNA), and HrpB as specified were incubated for 15 min at 37°C. Pi release was plotted as a function of input protein. (B) RNA preferences. Reaction mixtures (15  $\mu$ l) containing 50 mM Tris-HCl (pH 8.0), 1 mM DTT, 2 mM MgCl<sub>2</sub>, 1 mM [ $\gamma$ -<sup>32</sup>P] ATP, nucleic acids (either 80 ng/ $\mu$ l MS2, 100 ng/ $\mu$ l *P. aeruginosa* rRNA, 5  $\mu$ M R41, or 5  $\mu$ M D41), and HrpB (as specified) were incubated for 15 min at 37°C. Pi release was plotted as a function of input protein. Data are the average  $\pm$  SEMs from three independent experiments.

activity is strictly RNA dependent. Finally, we examined the effect of long-structured RNAs, namely MS2 (~3500-nts) and *P. aeruginosa* rRNA (for the preparation see Materials and Methods). Both are shown to be potent activators of the HrpB ATPase activity, displaying 83% and 67% of the activity with poly(A), respectively (Fig. 4B).

#### Deletion analysis defines a role of the CTE on HrpB RNA preferences

Two CTE deletion mutations HrpB<sub>1-702</sub> and HrpB<sub>1-628</sub> were designed to progressively truncate HrpB CTE as shown in Fig. 1B. We successfully expressed and purified both His<sub>10</sub>Smt3-tagged variants and the mobility during SDS-PAGE was consistent with the calculated size of 91, and 83 kDa, respectively (Fig. 5A). Subsequently, in order to test the CTE role in RNA recognition, we assessed RNA preferences of the two truncated variants. Both HrpB<sub>1-702</sub> and HrpB<sub>1-628</sub> retained similar ATPase activity as wild-type HrpB in presence of poly(A) (75% and 69% of the wild-type activity, respectively); signifying that the C-terminal 198-aa extension was dispensable for catalytic activity *in vitro* (Fig. 5B). In contrast to wild-type HrpB, no RNA-independent ATPase activity was detected at the enzyme concentration tested (Fig. 5B). We next compared the RNA preferences of both truncations by using different RNAs as cofactor. We found that both truncated proteins (HrpB<sub>1-702</sub> and HrpB<sub>1-628</sub>) possess similar ATPase activity as wild-type HrpB when the reaction mixture contains poly(C), poly(G), poly(U), and the 41-mer RNA. However, we found that the extent of phosphate release by HrpB<sub>1-702</sub> and HrpB<sub>1-628</sub> with the MS2 RNA was 20% and 23% of the activity with the wild-type HrpB (Fig. 5C). Similarly, we found that the level of HrpB<sub>1-702</sub> and HrpB<sub>1-628</sub> ATPase was also reduced in presence of *P. aeruginosa* rRNA when compared to the wild-type HrpB, although at a lower level than MS2 (46% and 39%, respectively). Surprisingly, these data show an involvement of the CTE in RNA recognition as they reveal that the CTE is crucial for the

stimulation of HrpB ATPase activity by MS2 or other structured RNAs (such as rRNA).

#### Role of the accessory domains on RNA preferences

We performed several attempts in order to express and purify variants of HrpB lacking one or more accessory domains (Fig. 1B, HrpB<sub>1-365</sub>, HrpB<sub>1-390</sub>, HrpB<sub>1-500</sub>, HrpB<sub>1-539</sub>, HrpB<sub>1-589</sub>). Only one variant that contained only the RecA1 and RecA2 domains, HrpB<sub>1-365</sub>, was produced with reasonable yield (Fig. 6A), all the others were insoluble. HrpB<sub>1-365</sub> catalyzes the release of Pi from [ $\gamma$ -<sup>32</sup>P] ATP in the presence of poly(A) and we found that the extent of ATP hydrolysis is proportional to enzyme concentration; 65% of the ATP substrate was hydrolysed at 20 ng/ $\mu$ l of protein (Fig. 6B). A specific activity of 0.0312 nmol of ATP hydrolysed per ng of protein in 15 min was calculated from the slope of the titration curve in the linear range. (This value translates into a turnover number of 114 min<sup>-1</sup>). Omission of poly(A) from the ATPase reaction mixture reduced ATP hydrolysis by about 4-fold. Treatment with RNase A did not reduce the HrpB<sub>1-365</sub> phosphohydrolase activity in the absence of poly(A) (data not shown), indicating that the observed ATPase activity of HrpB<sub>1-365</sub> is RNA independent. This is intrinsic to the recombinant protein as insofar the ATPase activity of the K33A mutation was less than 1% of the activity of HrpB<sub>1-365</sub> in both the presence and absence of poly(A). We next assessed the RNA substrate specificity of HrpB<sub>1-365</sub> (Fig. 6C). The salient finding was that poly(U), which was unable to stimulate efficiently the ATPase of wild-type HrpB (only 20% of the activity observed with poly(A); Fig. 4A) was able to stimulate HrpB<sub>1-365</sub> ATPase at the same degree as poly(A). Similar to HrpB<sub>1-702</sub> and HrpB<sub>1-628</sub>, the HrpB<sub>1-365</sub> ATPase activity stimulation by MS2 and rRNA was poor, confirming the CTE importance for recognition of these RNAs. Altogether, HrpB accessory domains strictly restrain the stimulatory action of HrpB ATPase at RNAs and inhibit poly(U) RNA recognition.

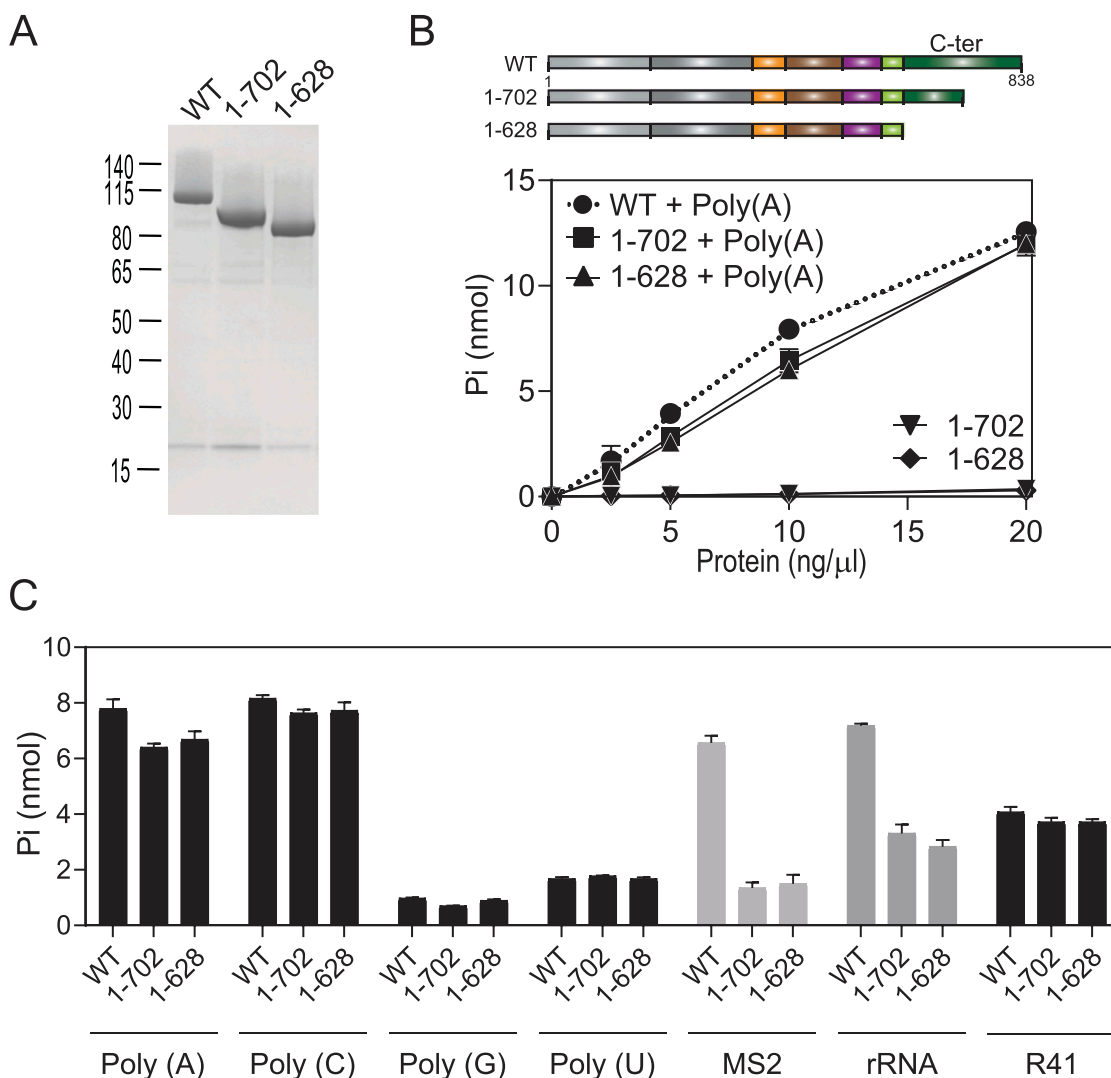


**Figure 5. HrpB C-terminal deletion (1–702) and (1–628).** (A) HrpB purification. Aliquots (2.5 μg) of the nickel-agarose preparations of wild-type (WT) HrpB, deletion mutant HrpB (1–702), and deletion mutant HrpB (1–628) were analysed by SDS-PAGE. A Coomassie Blue-stained gel is shown. The positions and sizes (in kDa) of marker proteins are indicated on the left. (B) ATPase activity. Reaction mixtures (15 μl) containing 50 mM Tris-HCl (pH 8.0), 1 mM DTT, 2 mM MgCl<sub>2</sub>, 1 mM [γ-<sup>32</sup>P] ATP, 250 ng/μl Poly(A) (or No RNA), and WT or mutant proteins as specified were incubated for 15 min at 37°C. Pi release was plotted as a function of input protein. (C) RNA specificity. Reaction mixtures (15 μl) containing 50 mM Tris-HCl (pH 8.0), 1 mM DTT, 2 mM MgCl<sub>2</sub>, 1 mM [γ-<sup>32</sup>P] ATP, and 250 ng/μl polyribonucleotide or RNA as specified (250 ng/μl of each polyribonucleotide, 80 ng/μl MS2, 100 ng/μl *P. aeruginosa* rRNA, and 5 μM R41) and 10 ng/μl of WT HrpB were incubated for 15 min at 37°C. The extends of Pi release are plotted. (B and C) Data are the average ± SEMs from three independent experiments.

### HDX-MS reveals the HrpB regions involved in RNA recognition

The biochemical characterization of HrpB shows that whereas both poly(A) and MS2 stimulate efficiently the ATPase activity of full-length HrpB (Fig. 4), the latter fails to activate efficiently HrpB CTE deleted variants (Fig. 5). In addition, work on the RecA-only variant indicated an involvement of accessory domains in RNA discrimination. In order to identify more precisely HrpB sites involved in RNA recognition in an unbiased manner, we performed hydrogen-deuterium exchange coupled to mass spectrometry (HDX-MS) experiments of purified *Pa*HrpB in presence and absence of poly(A) and MS2 RNAs. HDX-MS is a powerful method that looks at protein dynamics in solution based on the rate of exchange of protein amide protons with the solvent [28,29]. Poly(A) and MS2 do not share sequence similarities and have divergent structures, therefore they

represent good candidates to assess whether and how HrpB discriminates among different types of RNA molecules.

HrpB proteins, in absence and presence of RNA, were incubated with deuterated buffer over several time intervals (30 s, 300 s, 1800 s and 3600 s) before quenching of the reaction at low pH and temperature (Supplementary Figure S7). Deuterium incorporation was quantified by digesting the samples with pepsin and UPLC-MS analysis. In total, 189 *Pa*HrpB peptides were identified and characterized in all three conditions, representing a sequence coverage of 96% (Supplementary Figure S8 and Supplementary Table S4). HDX rates for HrpB apo state and HrpB in presence of RNA (poly(A) or MS2) were calculated for each peptide and differences were considered significant when both % deuteration and number of deuterons were exceeding the threshold (Supplementary Table S4).

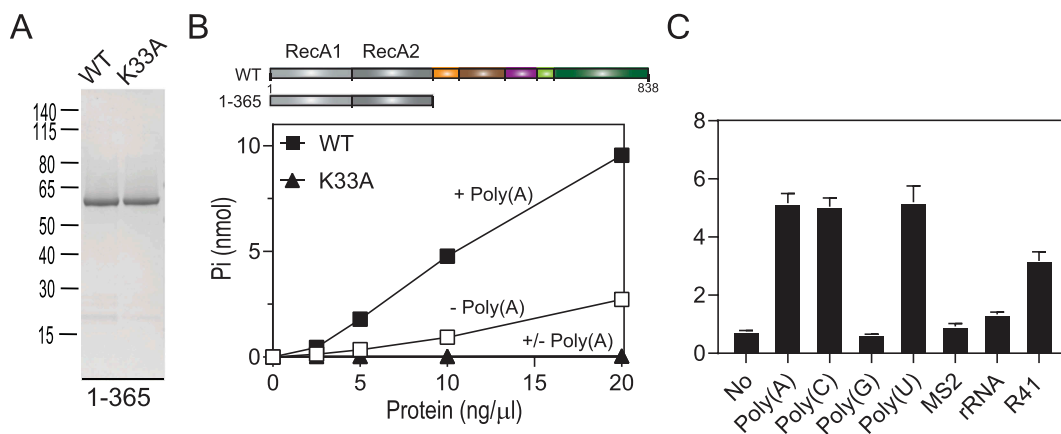


**Figure 6. HrpB deletion mutant (1–365) and its ATPase activity.** HrpB (1–365) purification. Aliquots (2.5 μg) of the nickel-agarose preparations of the deletion mutant (1–365) and mutant K33A were analysed by SDS-PAGE. A Coomassie Blue-stained gel is shown. The positions and sizes (in kDa) of marker proteins are indicated on the left. (A) Protein titration. Reaction mixtures (15 μl) containing 50 mM Tris-HCl (pH 8.0), 1 mM DTT, 2 mM MgCl<sub>2</sub>, 1 mM [ $\gamma$ -<sup>32</sup>P] ATP, 250 ng/μl Poly(A) (or No RNA), and deletion mutant (1–365) or K33A mutant proteins as specified were incubated for 15 min at 37°C. Pi release was plotted as a function of input protein. (C) RNA specificity. Reaction mixtures (15 μl) containing 10 ng/μl of WT HrpB, 50 mM Tris-HCl (pH 8.0), 1 mM DTT, 2 mM MgCl<sub>2</sub>, 1 mM [ $\gamma$ -<sup>32</sup>P] ATP, nucleic acid (or no RNA) as specified were incubated for 15 min at 37°C. The extends of Pi release are plotted. (B and C) Data are the average  $\pm$  SEMs from three independent experiments.

Overall, we identified several regions within PaHrpB that exhibit increased or reduced exchange rate in the presence of either one or both types of RNAs (Fig. 7 and Supplementary Figure S9). These were mapped on the PaHrpB structure as colour-coded surfaces (Fig. 8 and Supplementary Figure S10). As expected, motifs Ia, Ib, Ic within the RecA1 domain and motifs IV, IVa, and V within the RecA2 domain are protected from deuteration over the time, in presence of both RNAs (Fig. 8). These results are in agreement with data from the literature that identify those motifs to be responsible for RNA binding in the catalytic core of RNA helicases [2,5,11]. Residues 8–25 in the RecA1 domain, upstream of the motif I were also protected from deuteration in the presence of poly(A), while with MS2 the difference was less significant.

Interestingly, residues 609–627 within the CON domain exhibited an RNA-induced increase in deuterium uptake, both with poly(A) and MS2 RNAs (Fig. 8). The increase was more pronounced in presence of MS2, where a significant increase in deuterium uptake was also observed for residues 590–599 between the end of the OB domain and the beginning of the CON domain. This increase in deuterium exchange rate likely represents conformational rearrangements triggered by RNA binding.

Finally, peptides within the accessory domains and the CTE were protected from exchange specifically by the MS2 RNA (residues 449–494 within the HB domain, 559–578 within the OB domain, and 757–763 within the CTE) (Fig. 8). Considering that these regions were not affected by poly(A), these results confirm the biochemical data on the involvement of the accessory domains and CTE in the protein recognition of long structured RNA. It remains to be established whether these regions directly contact RNA or are remodelled as a consequence of RNA binding elsewhere on the surface of the protein.

## Discussion

In eukaryotes, DEXH-box helicases have been shown to regulate many essential processes of RNA metabolism [20,30]. In prokaryotes, their role and mechanism of action is just starting to be deciphered. Recently, the structure of HrpB DEXH-box protein from *E. coli* revealed the presence of several domains additional to the RecA-like catalytic core, namely three eukaryotic-like accessory domains (WH, HB, and OB domain) and a unique C-terminal extension (CTE) [18,19]. However, the function of these auxiliary domains has not been investigated. Here, we characterize HrpB from the Gram-negative opportunistic pathogen *P. aeruginosa* with the aim of assessing the role of auxiliary domains in respect to protein-RNA interaction.

We used the HrpB ATPase activity as a proxy to probe its RNA preferences and we found that the single-stranded RNAs poly(A) and poly(C) were the strongest inducers, while poly(U) and poly(G) were not effective activators (13% and 19% of the activity with poly(A) substrate, respectively). Most RNA helicases do not show RNA substrate specificity *in vitro* [6,7,31]; therefore, it was surprising to observe that poly(G) and poly(U) are unable to stimulate HrpB ATPase activity. However, it is not unprecedented as SrmB, a DEAD-box helicase from *E. coli*, has been also shown to be stimulated by poly(A) and poly(C), but not by poly(U) [32]. Importantly, homopolyribonucleotides differ not only by their primary RNA sequence but also by their secondary and higher order structures [33]. Thus, it is more likely that HrpB would prefer some RNA structures over others. For example, under physiological conditions poly(G) adopts quadruplex structures that could impair the recognition by HrpB [33,34]. Of note, poly(I) does not form quadruplexes and indeed stimulates HrpB ATPase similarly to poly(A) (data not shown). Likewise, poly(U) could be a poor activator of HrpB ATPase because it occurs as a single-stranded molecule adopting random coils, whereas poly(A) and



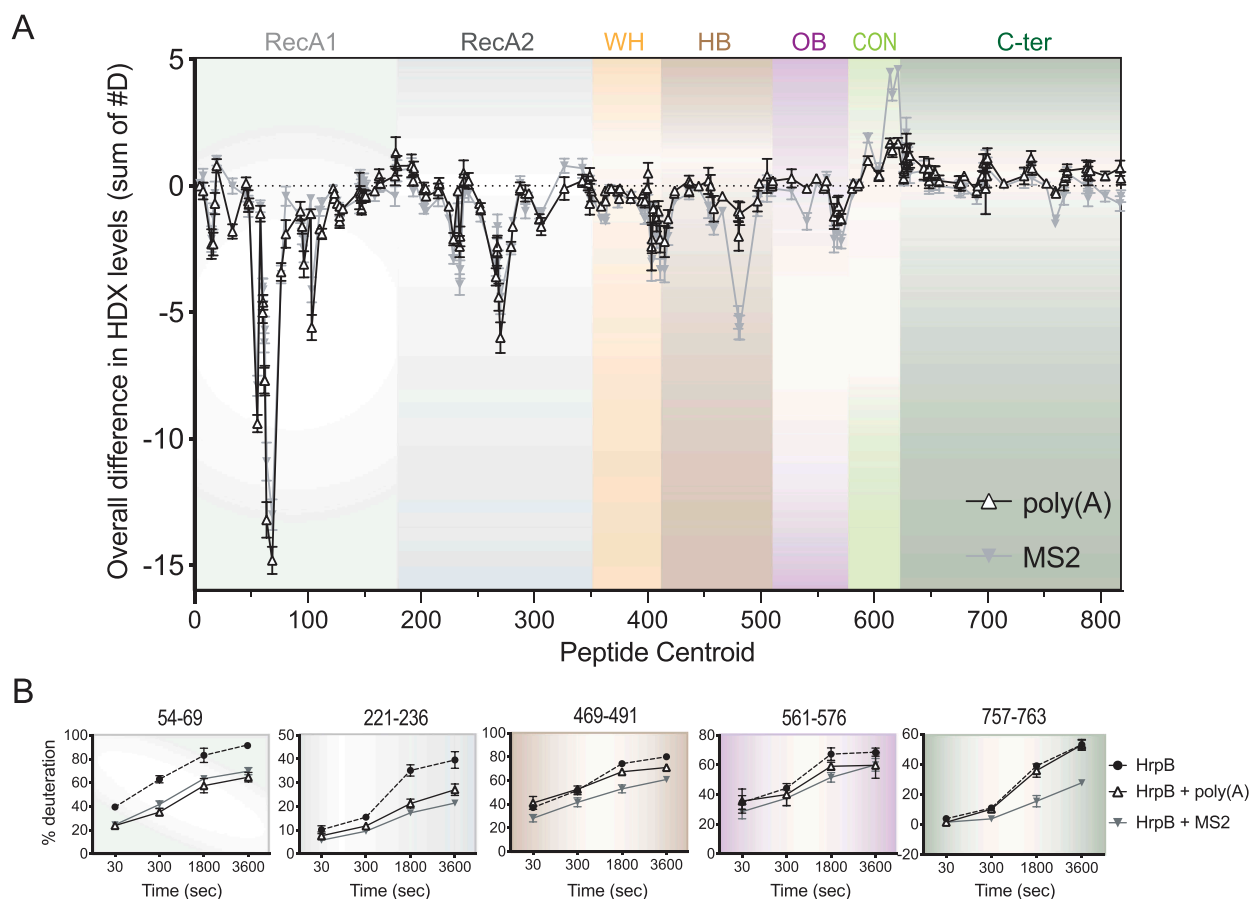


**Figure 7. Identification of HrpB RNA responsive regions by HDX-MS.** (A) Linear plot highlighting HDX changes in HrpB induced by poly(A) (white triangles) or MS2 (grey triangles) as a function of the central residue number for each peptide (x-axis). Coloured regions correspond to the RecA-like, WH, HB, OB, CON, and C-ter domains as in Fig. 1. (B) Deuterium uptake plots (% deuteration  $\pm$  standard deviation) over time of some HrpB regions. Residue number is indicated on top of each graph. Graph background is coloured according to the domain to which they belong, according to panel A and Fig. 1.

poly(C) good activator because they exist as single-stranded molecules with ordered helical and coiled structures [33].

Concomitantly, MS2 and rRNA are strong activators of HrpB activity but, contrarily to poly(A) and poly(C), only if HrpB CTE was present. MS2 is a  $\sim$  3500-nt RNA that folds into a complex structure with several hairpins linked to each other or bound by secondary interactions, and with some single-stranded segments [35]. We therefore reasoned that long single-stranded RNA and structured RNA could not interact with HrpB the same way. Given the high diversity and complexity of heteropolymeric and MS2/rRNAs, a study of their interaction with HrpB would have been challenging by classical methods. Instead, the use of HDX-MS allowed us to get valuable insights into HrpB-RNAs interaction. The HDX-MS technique has been used previously to map protein-protein interaction sites [36], protein-lipid interfaces [37], protein-RNA [38] and small molecule binding sites [39]. To our knowledge, the only other protein carrying a RecA-like core on which the technique has been applied was the RIG-I RNA sensor [40,41]. Here, HDX-MS data revealed that HrpB auxiliary domains recognize differently poly(A) and MS2 RNAs. By combining the HDX-MS data

with enzymatic activity experiments on HrpB truncations, we then confirmed their contribution to HrpB RNA recognition.

### RNA responsive-motifs in DEXH-box proteins

In general, SF2 helicases bind to nucleic acid ligands using a conserved surface, which contains signature motifs Ia, Ib, and Ic (when present) in RecA1 and motif IV, IVa, and V in RecA2. Our HDX-MS analysis validated those motifs as 'RNA responsive elements' for the two tested RNAs poly(A) and MS2 (Fig. 5, 6 and Supplementary Table S4).

In the structure of many DEXH-box helicases, e.g. Prp43, the RecA-like domains and the accessory domains appear to form a tunnel within which RNA binding occurs [7]. In HrpB, the accessory domains (precisely residues 449–494 in HB domain and residues 559–578 in OB domain) seem to be involved specifically on MS2 recognition, while they are unaffected by poly(A). In addition, we also found an involvement of CTE residues (amino acids 757–763) in MS2 interaction. Alignment of bacterial HrpB sequences highlights these residues to be highly conserved (Supplementary Figure S1). As a reminder, when those residues were deleted (in HrpB<sub>1-628</sub> and HrpB<sub>1-702</sub>) the protein loses 5- and

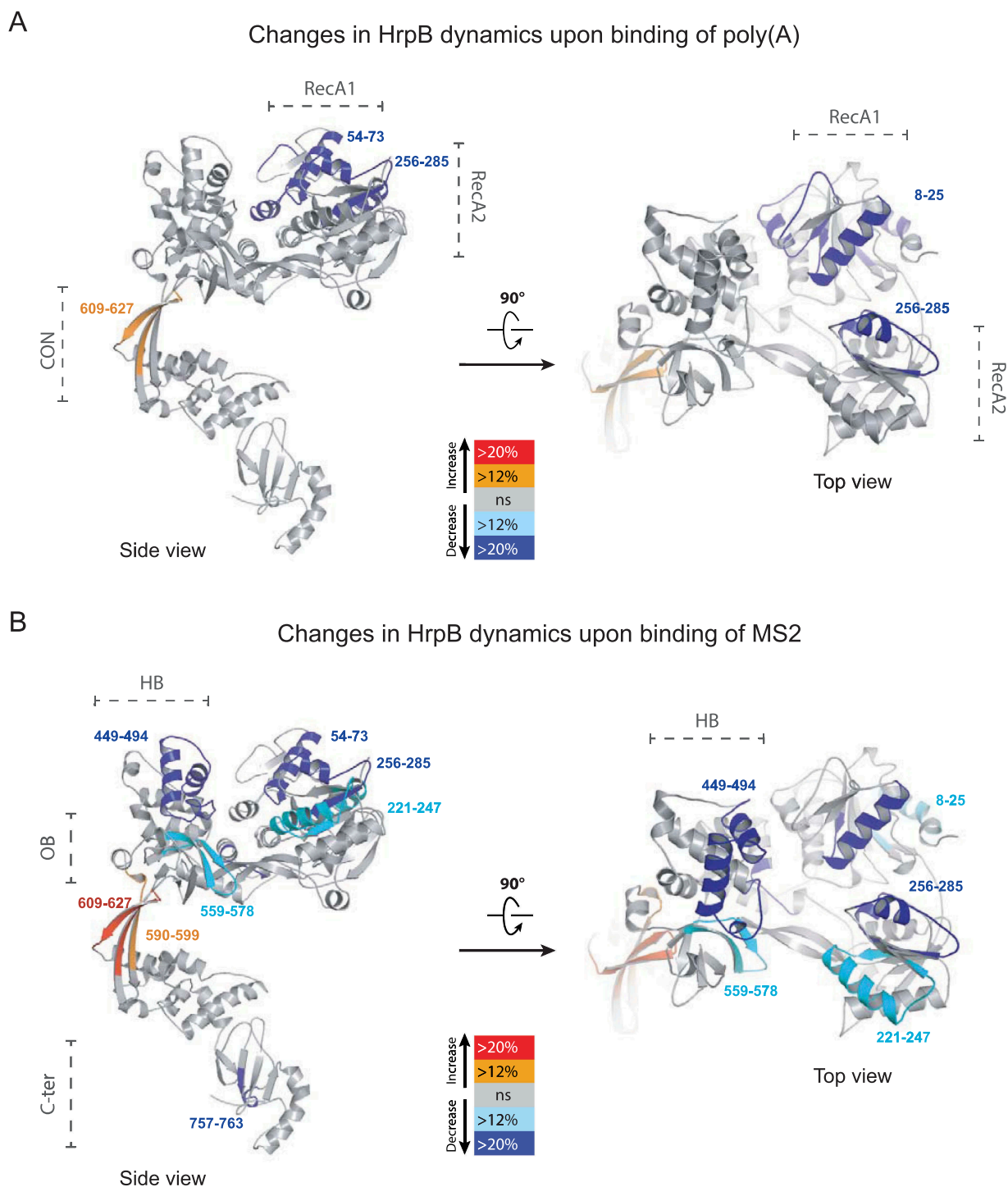


**Figure 8. Mapping of RNA responsive region on HrpB structure.** Peptides with significant changes in presence of poly(A) (A) or MS2 (B) are coloured on the ribbon diagram of the *P. aeruginosa* HrpB structure (Supplementary Figure S9) using PyMOL and according to the colour scheme shown (red and orange for increased hydrogen-deuterium exchange [HDX], cyan and blue for decreased HDX).

2-fold activity with MS2 and rRNA, respectively, while no significant changes are detected with poly(A) or other RNAs (Fig. 5). Compared to CTE truncated variants, deletion of the accessory domains does not impact further the MS2 and rRNA dependent stimulation of HrpB (Fig. 6). Altogether, our finding indicates that residues 703–838 are necessary requirements for MS2 and rRNA recognition by HrpB. In *E. coli*, CTE truncations of HrpB were shown to have only a marginal impact on the ATPase activity [18]. This is not in contrast with our data as we notice that in Pietrzyk-

Brzezinska *et al.* the ATPase assays were performed in presence of short single-stranded RNAs (26-nt) and we observed the same trend with 40-nt RNAs (Fig. 5). Thus, the use of long RNAs (which has never been tested so far) allowed us to unveil the role of HrpB auxiliary domains on RNA recognition. It has to be mentioned, though, that the C-terminal region of HrpB is largely negatively charged; thus, it has been proposed to be involved in HrpB interaction with other proteins. Our data do not exclude this hypothesis and it is still possible that HrpB is part

of a bigger RNP complex, interacting both with RNAs and RBPs. In yeast, Prp43 associates with the G-patch protein Ntr1, and Ntr2, which together form the NTR complex [42–44]. Ntr1 binds to the C-terminal domain of Prp43 and thereby stimulates Prp43's ATPase and RNA helicase activity [45,46].

Finally, increased dynamics of the CON domain in the presence of both poly(A) and MS2 highlights conformational changes of HrpB upon RNA-binding. Conformational changes of Prp43 in presence of U7 RNA were shown to induce an opening of the RNA-binding tunnel and a disruption of the interaction between two  $\beta$ -hairpin loops from the RecA2 domain and the OB domain, which are crucial for the helicase activity of Prp43 [7]. Up to now, any attempt to show HrpB helicase activity has failed [18,19]. Since we observe a lower extent of CON domain exposure with poly(A) in respect to MS2 RNA, it is thus possible that, if any, the helicase activity might necessitate specific type of RNAs triggering the conformational change.

### RNA preferences of a DExH-box protein catalytic core

Few examples of minimal RNA helicases have been shown to exist in nature and they all belong to the DEAD-box family, like eIF4A-I or eIF4A-III [47]. Minimal helicases are instrumental in understanding the general mechanism of action of RecA-like domains and the contribution of auxiliary domains to the core activity. We were able to obtain the first minimal DExH-box protein by purifying an HrpB variant (HrpB<sub>1-365</sub>) that consists only of the catalytic core, i.e. the two RecA domains. We show here that the auxiliary domains of HrpB impact its RNA preferences. Compared to HrpB full-length, HrpB<sub>1-365</sub> gains a poly(U)-dependent ATPase activity (almost 5-fold increase when compared to HrpB full-length). Only the DExH-box helicase MLE has been reported to display an unusual specificity for uridines [6]. The residues of MLE that are forming uracil-specific contact are located mainly on the OB domain, except from residues R470 and R492 in the RecA1 domain [6]. The two stacking residues of MLE located in the RecA1 domain are also conserved in HrpB (R86/R470, R107/R492 in HrpB/MLE, respectively), while the ones mapping in the OB domain are missing (Supplementary Figure S2). Our hypothesis is that because of poly(U) disordered conformation (see above), accessory domains might hinder its access to the RNA-binding cleft formed by the two RecA domains. The rationale for MLE and other spliceosomal helicases which OB domain contains uracil-contacting residues has been given by their function in the context of uridine-rich small nuclear RNAs [6,48]. Comparing our work with MLE data indicates that uridine-specificity evolved exclusively in eukaryotic cells.

### Role of HrpB

In *X. citri*, HrpB has been shown to regulate bacterial sliding motility, biofilm formation, virulence, and within-host survival [22]. In *E. coli*, HrpB is not involved in any of these functions [18]. The biological function of HrpB in *P. aeruginosa*, like in *E. coli*, still needs to be revealed. In the literature, we find several examples of RNA helicases which

deletion does not lead to a loss in viability nor, in some instances, a distinct phenotype [49–51]. In bacteria, a well-known example is DbpA, a DEAD-box RNA helicase that binds and is specifically activated by 23S RNA [50,52]. Despite its function in ribosome assembly, a cold-sensitive slow growth phenotype could be observed only by overexpressing in *E. coli* a dominant negative DbpA point mutation (R331A), while growth of *dbpA* deleted strain in several media and conditions was shown to be similar to the wild-type [50,53]. Like for DbpA, HrpB loss could affect *P. aeruginosa* and *E. coli* growth only under yet undetermined conditions. Alternatively, other RNA helicases could mask the phenotypic consequences of *hrpB* deletion. HrpA is a second DExH-box protein that has been shown to affect *P. aeruginosa* response to azithromycin [54]. Little redundancy has been proposed for DEAD-box helicases [55–57]. Moreover, recent experiments performed in the laboratory indicate that deletion of *hrpB*, both in a wild-type and a  $\Delta$ *hrpA* genetic background, does not affect the parental strain resistance to azithromycin (data not shown). In the future, we plan to further investigate any epistasis and redundancy between *hrpA* and *hrpB* by an in-depth evaluation of *hrpA/hrpB* double mutant and cross-complementation. We will also focus on finding the natural RNA target(s) of HrpB (using RNA-immunoprecipitation assays) or interacting partner (through pull-down experiments), which could shed light on its biological function.

## Materials and methods

### Bacterial strains and culture conditions

The bacterial strains/plasmids and oligonucleotides used in the present study are listed in Supplementary Table S1 and S2, respectively. Growth was performed at 37°C in Luria-Bertani broth (LB) or agar (LA). When required, antibiotics were added at the following concentrations: 50  $\mu$ g/ml of kanamycin, 25  $\mu$ g/ml of tetracycline, and 34  $\mu$ g/ml of chloramphenicol for *E. coli* and 100  $\mu$ g/ml of tetracycline for *P. aeruginosa*.

### RNA substrates

R41 (5'GCGUCUUUACGGUGCUUAAAACAAAACAAAACA AAACAAA) and D41 (the same base sequence as R41 except T for U in DNA) were purchased from MicroSynth (PAGE purified quality). Poly(A), poly(U), poly(C), poly(G), and MS2 RNA was purchased from Sigma. *P. aeruginosa* total RNA (~90% rRNA) was extracted and purified from an O/N culture using phenol-chloroform extraction, treated with DNase I (Promega) two-three times to remove contaminating genomic DNA and re-purified again using phenol-chloroform. Eventual DNA contamination was tested by PCR with primers rpoD.fw and rpoD.rev (Supplementary Table S2).

### Constructions of plasmids and gene replacement mutants

DNA cloning and plasmid preparation were performed according to standard methods [58]. Restriction and DNA-modifying enzymes were used according to the instructions of

the manufacturers. All constructs were confirmed by sequencing prior to use.

For the inactivation of the *hrpB* gene in the *P. aeruginosa* PAO1 chromosome, a 330-bp fragment containing the upstream region and the first 50 codons of *hrpB* and a 460-bp fragment containing the *hrpB* terminator were amplified by PCR using the primer pairs pHrpB.1/2 and pHrpB.3/4, respectively. These products were cloned into the suicide vector pME3087, yielding plasmid pME3087 $\Delta$ *hrpB*. The plasmid, carried by *E. coli* DH5 $\alpha$ , was then introduced into *P. aeruginosa* PAO1 by triparental mating, using the helper strain *E. coli* HB101 (pRK2013). Merodiploids were resolved as previously described [59]. Deletion of the gene of interest was verified by PCR.

For the production of His<sub>10</sub>Smt3-HrpB in *E. coli* BL21 (DE3), the *hrpB* gene was amplified from *P. aeruginosa* genomic DNA (using plasmid pHrpB-Smt3.1 and pHrpB.rev) and cloned into pET28b10xHis-Smt3 between HindIII site at the start codon and an XhoI site 3' of stop codon. The resulting recombinant plasmid pSmt3-HrpB encoded HrpB with an N-terminal cleavable 10xHis-Smt3 tag. For site-directed mutagenesis, the pSmt3-HrpB plasmid was used as template and it was amplified with mutated primers listed in Table S2. Template was then digested by DpnI and the mutated plasmid introduced into *E. coli* [58]. The mutation was confirmed by sequencing.

### HrpB purification

The pET28-His<sub>10</sub>Smt3-HrpB plasmids were transformed into *E. coli* BL21 (DE3). Cultures (500 ml) derived from single transformants were grown at 37°C in LB medium containing kanamycin until the OD<sub>600</sub> reached 0.6. The cultures were adjusted to 0.2 mM IPTG and 2% (v/v) ethanol and incubation was continued for 20 h at 17°C. Cells were harvested by centrifugation and stored at -80°C. All subsequent procedures were performed at 4°C. Thawed bacteria were resuspended in 25 ml of buffer A (50 mM Tris-HCl, pH 8.0, 200 mM NaCl, 10% glycerol) and supplemented with one tablet of protease inhibitor cocktail (Roche). The suspension was adjusted to 0.1 mg/ml lysozyme and incubated on ice for 30 min. Imidazole was added to a final concentration of 10 mM and the lysate was sonicated to reduce viscosity. Insoluble material was removed by centrifugation. The soluble extracts were mixed for 30 min with 3 ml of Ni<sup>2+</sup>-NTA-agarose (Qiagen) that had been equilibrated with buffer A containing 10 mM imidazole. The resins were recovered by centrifugation, resuspended in buffer A with 10 mM imidazole, and poured into columns. The column was washed with 15 ml aliquots of 20 mM imidazole in buffer A and then eluted stepwise with 5 ml aliquots of buffer A containing 50, 100, 250, and 500 mM imidazole, respectively. The elution profiles were monitored by SDS-PAGE (not shown; 250 mM imidazole fraction is shown in Fig. 2A). The recombinant protein His<sub>10</sub>Smt3-HrpB was recovered predominantly in the 250 mM imidazole eluate fraction. The protein concentration of the 250 mM imidazole eluate fraction was determined using the Bio-Rad dye reagent with BSA as the standard. HrpB mutated variants were produced and purified as described above for the wild-type HrpB.

### ATPase reaction

Reaction mixtures (15  $\mu$ l) containing 50 mM Tris-HCl, pH 8.0, 2 mM DTT, 2 mM MgCl<sub>2</sub>, 1 mM [ $\gamma$ -<sup>32</sup>P] ATP, RNA, and enzyme as specified were incubated for 15 min at 37°C. The reactions were quenched by adding 3.8  $\mu$ l of 5 M formic acid. Aliquots (2  $\mu$ l) were applied to a polyethylenimine(PEI)-cellulose F thin layer chromatography (TLC) plates (Merck), which were developed using 1 M formic acid and 0.5 M LiCl. Pi release was quantitated by scanning the chromatogram with laser Scanner Typhoon FLA 7000 (General Electric).

### Phenotypic assays

Liquid growth assays were performed in 96-well plates each containing 200  $\mu$ l of LB and cell density (OD 600) was measured with a Synergy H1 plate reader (Biotek). Spot assays were performed by spotting 10  $\mu$ l of serial dilutions of cultures (at initial OD<sub>600</sub> of 1.0) on LB plates incubated at 16°C or at 37°C or supplemented with either 0.5 M NaCl or 2 mM H<sub>2</sub>O<sub>2</sub>.

Quantification of biofilm formation was performed in 24-well polystyrene microtiter plates or glass tubes as previously described [60]. The plates were incubated for either 6 hours (hrs) in static conditions (attachment) or for 18 h at 180 rpm (biofilm) at 37°C. Cells were stained with 0.1% crystal violet solution and the dye bound was solubilized with 96% (v/v) ethanol. The absorption was photometrically measured at 600 nm (OD<sub>600</sub>). Congo-red staining assay was performed on tryptone (10 g/l) agar (1%) plates supplemented with 40  $\mu$ g/ml Congo red and 20  $\mu$ g/ml Coomassie brilliant blue.

Motility assays were performed essentially as previously described [60]. Swim assays were carried out on 10 g/L tryptone, 5 g/L NaCl, 0.3% agar (Merck) plates, twitch assays on 1% LB agar plates and swarm assays on plates containing 0.5% (wt/vol) Difco bacto-agar with 8 g/litre Difco nutrient broth and 5 g/litre glucose. Pictures were taken from plates of five independent experiments and the ImageJ software (NIH) was used to determine the area of the plate surface covered by the bacteria.

The wax moth model *Galleria mellonella* was used for *in vivo* virulence assay, as previously described [61]. Briefly, overnight cultures were diluted 1:100 and sub-cultured (3 ml LB) at 37°C until exponential phase (3 h). Bacterial cells (OD<sub>600</sub> = 1.0) were washed with PBS three times. The samples were serially diluted (up to 10<sup>-7</sup>) and a 10  $\mu$ l volume of the dilutions was spotted on LB agar and CFU counted the next day. A 10  $\mu$ l volume of the 10<sup>-7</sup> dilution for the wild-type and  $\Delta$ *hrpB* mutant strain (dilution of 10<sup>-3</sup> was used for the PAO1*hfq*- strain) was injected into the last abdominal proleg of ten larvae per sample. An additional ten larvae were injected with PBS as negative control. Larvae mortality was monitored every 2 h from 16- to 40-h post-infection (larvae are considered dead when they turn black and do not respond to tapping).

All data are mean values of three independent samples  $\pm$  standard deviation.

## HDX-MS

HDX-MS experiments were performed at the UniGe Protein Platform (University of Geneva, Switzerland). A schematic of how HDX-MS reactions were carried-out is presented in Supplementary Figure 7. Details of reaction conditions and all data are presented in Tables S3 and S4. HDX reactions were done in 50  $\mu$ l volumes with a final protein concentration of 6.3  $\mu$ M of His<sub>10</sub>Smt3-HrpB. Briefly, 63 picomoles of protein were incubated with either i) no RNA, ii) poly(A) (1  $\mu$ g/ $\mu$ l) or iii) MS2 RNA (0.7  $\mu$ g/ $\mu$ l) in 10  $\mu$ l final volume of binding buffer (10 mM Tris, pH 8.0, 2 mM MgCl<sub>2</sub>) for 1 h on ice before the reaction.

Deuterium exchange reaction was initiated by adding 40  $\mu$ l of D<sub>2</sub>O exchange buffer (10 mM Tris pH 8/2 mM MgCl<sub>2</sub> in D<sub>2</sub>O) to the 10  $\mu$ l protein-RNA mixture. Reactions were carried out on ice for 4 incubation times (30 s, 300 s, 1800 s, 3600 s) and terminated by the sequential addition of 20  $\mu$ l of ice-cold quench buffer 1 (3 M Guanidium-HCl (Gdn-HCl) /0.1 M NaH<sub>2</sub>PO<sub>4</sub> pH 2.5/1% Formic Acid). Samples were immediately frozen in liquid nitrogen and stored at  $-80^{\circ}$ C for up to 2 weeks. All experiments were repeated in triplicate (Supplementary Table S3).

To quantify deuterium uptake into the protein, protein samples were thawed and injected in a UPLC system immersed in ice. The protein was digested via two immobilized pepsin columns (Thermo #23,131), and peptides were collected onto a VanGuard precolumn trap (Waters). The trap was subsequently eluted, and peptides separated with a C18, 300Å, 1.7  $\mu$ m particle size Fortis Bio 100  $\times$  2.1 mm column over a gradient of 8–30% buffer C over 20 min at 150  $\mu$ l/min (Buffer B: 0.1% formic acid; buffer C: 100% acetonitrile). Mass spectra were acquired on an Orbitrap Velos Pro (Thermo), for ions from 400 to 2200 m/z using an electrospray ionization source operated at 300°C, 5 kV of ion spray voltage. Peptides were identified by data-dependent acquisition after MS/MS and data were analysed by Mascot. All peptides analysed are shown in Figure S8. Deuterium incorporation levels were quantified using HD examiner software (Sierra Analytics), and quality of every peptide was checked manually. Results are presented as percentage of maximal deuteration using a fully deuterated sample prepared by incubating the protein for 1 h in 1 M Gdn-HCl before incubation for 6 h in deuterated buffer. Changes in deuteration level between two states were considered significant if >12% and >0.6 Da and  $p < 0.05$  (unpaired t-test).

## Structure modelling

The full-length *P. aeruginosa* HrpB structure was modelled based on the *E. coli* HrpB structure (PDB code: 6EUD and 6HEG) using HHPred (<http://toolkit.tuebingen.mpg.de/hhpred>) [62].

## Acknowledgements

We are grateful to Patrick Linder for critical reading of the manuscript. We thank the Proteomics Core Facility at the University of Geneva for assistance with HDX-MS data acquisition.

## Disclosure statement

No potential conflict of interest was reported by the authors.

## Funding

This work was supported by a Swiss National Science Foundation Ambizione grant (SNSF) [PZ00P3\_174063 to M.V.] and a grant from the Novartis Foundation for medical-biological Research [grant number 18B105 to M.V.]; Novartis Stiftung für Medizinisch-Biologische Forschung [18B105]; SNSF [PZ00P3\_174063].

## ORCID

Johan Geiser  <http://orcid.org/0000-0003-0046-1723>

Oscar Vadas  <http://orcid.org/0000-0003-3511-6479>

Martina Valentini  <http://orcid.org/0000-0002-1948-8339>

## References

- [1] Sloan KE, Bohnsack MT. Unravelling the mechanisms of RNA helicase regulation. *Trends Biochem Sci.* 2018;43:237–250.
- [2] Jankowsky E, Fairman ME. RNA helicases—one fold for many functions. *Curr Opin Struct Biol.* 2007;17:316–324.
- [3] Singleton MR, Dillingham MS, Wigley DB. Structure and mechanism of helicases and nucleic acid translocases. *Annu Rev Biochem.* 2007;76:23–50.
- [4] Cordin O, Banroques J, Tanner NK, et al. The DEAD-box protein family of RNA helicases. *Gene.* 2006;367:17–37.
- [5] Fairman-Williams ME, Guenther UP, Jankowsky E. SF1 and SF2 helicases: family matters. *Curr Opin Struct Biol.* 2010;20:313–324.
- [6] Prabu JR, Muller M, Thomae AW, et al. Structure of the RNA helicase MLE reveals the molecular mechanisms for uridine specificity and RNA-ATP Coupling. *Mol Cell.* 2015;60:487–499.
- [7] Tauchert MJ, Fourmann JB, Luhrmann R, et al. Structural insights into the mechanism of the DEAH-box RNA helicase Prp43. *Elife.* 2017;6:e21510.
- [8] Schmitt A, Hamann F, Neumann P, et al. Crystal structure of the spliceosomal DEAH-box ATPase Prp2. *Acta Crystallogr D Struct Biol.* 2018;74:643–654.
- [9] Galej WP, Wilkinson ME, Fica SM, et al. Cryo-EM structure of the spliceosome immediately after branching. *Nature.* 2016;537:197–201.
- [10] Fica SM, Oubridge C, Galej WP, et al. Structure of a spliceosome remodelled for exon ligation. *Nature.* 2017;542:377–380.
- [11] He Y, Andersen GR, Nielsen KH. Structural basis for the function of DEAH helicases. *EMBO Rep.* 2010;11:180–186.
- [12] Bertram K, Agafonov DE, Liu WT, et al. Cryo-EM structure of a human spliceosome activated for step 2 of splicing. *Nature.* 2017;542:318–323.
- [13] Cordin O, Hahn D, Beggs JD. Structure, function and regulation of spliceosomal RNA helicases. *Curr Opin Cell Biol.* 2012;24:431–438.
- [14] Schutz P, Wahlberg E, Karlberg T, et al. Crystal structure of human RNA helicase A (DHX9): structural basis for unselective nucleotide base binding in a DEAD-box variant protein. *J Mol Biol.* 2010;400:768–782.
- [15] He Y, Staley JP, Andersen GR, et al. Structure of the DEAH/RHA ATPase Prp43p bound to RNA implicates a pair of hairpins and motif Va in translocation along RNA. *RNA.* 2017;23:1110–1124.
- [16] Wagner JD, Jankowsky E, Company M, et al. The DEAH-box protein PRP22 is an ATPase that mediates ATP-dependent mRNA release from the spliceosome and unwinds RNA duplexes. *Embo J.* 1998;17:2926–2937.
- [17] Walbott H, Mouffok S, Capeyrou R, et al. Prp43p contains a processive helicase structural architecture with a specific regulatory domain. *Embo J.* 2010;29:2194–2204.
- [18] Pietrzyk-Brzezinska AJ, Absmeier E, Klauk E, et al. Crystal structure of the Escherichia coli DExH-Box NTPase HrpB. *Structure.* 2018;26:1462–1473.e1464.

- [19] Xin BG, Chen WF, Rety S, et al. Crystal structure of Escherichia coli DEAH/RHA helicase HrpB. *Biochem Biophys Res Commun.* 2018;504:334–339.
- [20] Redder P, Hausmann S, Khemici V, et al. Bacterial versatility requires DEAD-box RNA helicases. *FEMS Microbiol Rev.* 2015;39:392–412.
- [21] Winsor GL, Van Rossum T, Lo R, et al. Pseudomonas genome database: facilitating user-friendly, comprehensive comparisons of microbial genomes. *Nucleic Acids Res.* 2009;37:D483–488.
- [22] Granato LM, Picchi SC, Andrade Mde O, et al. The ATP-dependent RNA helicase HrpB plays an important role in motility and biofilm formation in Xanthomonas citri subsp. citri. *BMC Microbiol.* 2016;16:55.
- [23] Walker JE, Saraste M, Runswick MJ, et al. Distantly related sequences in the alpha- and beta-subunits of ATP synthase, myosin, kinases and other ATP-requiring enzymes and a common nucleotide binding fold. *Embo J.* 1982;1:945–951.
- [24] Tanner NK, Cordin O, Banroques J, et al. The Q motif: a newly identified motif in DEAD box helicases may regulate ATP binding and hydrolysis. *Mol Cell.* 2003;11:127–138.
- [25] Hanson PI, Whiteheart SW. AAA+ proteins: have engine, will work. *Nat Rev Mol Cell Biol.* 2005;6:519–529.
- [26] Tanaka N, Schwer B. Characterization of the NTPase, RNA-binding, and RNA helicase activities of the DEAH-box splicing factor Prp22. *Biochemistry.* 2005;44:9795–9803.
- [27] Tanaka N, Schwer B. Mutations in PRP43 that uncouple RNA-dependent NTPase activity and pre-mRNA splicing function. *Biochemistry.* 2006;45:6510–6521.
- [28] Kochert BA, Jacob RE, Wales TE, et al. Hydrogen-deuterium exchange mass spectrometry to study protein complexes. *Methods Mol Biol.* 2018;1764:153–171.
- [29] Mayne L. Hydrogen exchange mass spectrometry. *Methods Enzymol.* 2016;566:335–356.
- [30] Robert-Paganin J, Rety S, Leulliot N. Regulation of DEAH/RHA helicases by G-patch proteins. *Biomed Res Int.* 2015;(2015):931857.
- [31] Boneberg FM, Brandmann T, Kobel L, et al. Molecular mechanism of the RNA helicase DHX37 and its activation by UTP14A in ribosome biogenesis. *Rna.* 2019;25:685–701.
- [32] Bizebard T, Ferlenghi I, Iost I, et al. Studies on three E. coli DEAD-box helicases point to an unwinding mechanism different from that of model DNA helicases. *Biochemistry.* 2004;43:7857–7866.
- [33] Zarudnaya MI, Kolomiets IM, Potyahaylo AL, et al. Structural transitions in poly(A), poly(C), poly(U), and poly(G) and their possible biological roles. *J Biomol Struct Dyn.* 2019;37:2837–2866.
- [34] Shin YA. Interaction of metal ions with polynucleotides and related compounds. XXII. Effect of divalent metal ions on the conformational changes of polyribonucleotides. *Biopolymers.* 1973;12:2459–2475.
- [35] Fiers W, Contreras R, Duerinck F, et al. Complete nucleotide sequence of bacteriophage MS2 RNA: primary and secondary structure of the replicase gene. *Nature.* 1976;260:500–507.
- [36] Shukla AK, Westfield GH, Xiao K, et al. Visualization of arrestin recruitment by a G-protein-coupled receptor. *Nature.* 2014;512:218–222.
- [37] Vadas O, Dbouk HA, Shymanets A, et al. Molecular determinants of PI3Kgamma-mediated activation downstream of G-protein-coupled receptors (GPCRs). *Proc Natl Acad Sci U S A.* 2013;110:18862–18867.
- [38] Gonzalez GM, Hardwick SW, Maslen SL, et al. Structure of the Escherichia coli ProQ RNA-binding protein. *RNA.* 2017;23:696–711.
- [39] Masson GR, Maslen SL, Williams RL. Analysis of phosphoinositide 3-kinase inhibitors by bottom-up electron-transfer dissociation hydrogen/deuterium exchange mass spectrometry. *Biochem J.* 2017;474:1867–1877.
- [40] Zheng J, Wang C, Chang MR, et al. HDX-MS reveals dysregulated checkpoints that compromise discrimination against self RNA during RIG-I mediated autoimmunity. *Nat Commun.* 2018;9:5366.
- [41] Zheng J, Yong HY, Panutdaporn N, et al. High-resolution HDX-MS reveals distinct mechanisms of RNA recognition and activation by RIG-I and MDA5. *Nucleic Acids Res.* 2015;43:1216–1230.
- [42] Boon KL, Auchynnikava T, Edwalds-Gilbert G, et al. Yeast ntr1/spp382 mediates prp43 function in postspliceosomes. *Mol Cell Biol.* 2006;26:6016–6023.
- [43] Pandit S, Lynn B, Rymond BC. Inhibition of a spliceosome turnover pathway suppresses splicing defects. *Proc Natl Acad Sci U S A.* 2006;103:13700–13705.
- [44] Tsai RT, Tseng CK, Lee PJ, et al. Dynamic interactions of Ntr1-Ntr2 with Prp43 and with U5 govern the recruitment of Prp43 to mediate spliceosome disassembly. *Mol Cell Biol.* 2007;27:8027–8037.
- [45] Tanaka N, Aronova A, Schwer B. Ntr1 activates the Prp43 helicase to trigger release of lariat-intron from the spliceosome. *Genes Dev.* 2007;21:2312–2325.
- [46] Christian H, Hofele RV, Urlaub H, et al. Insights into the activation of the helicase Prp43 by biochemical studies and structural mass spectrometry. *Nucleic Acids Res.* 2014;42:1162–1179.
- [47] Rogers GW Jr., Richter NJ, Merrick WC. Biochemical and kinetic characterization of the RNA helicase activity of eukaryotic initiation factor 4A. *J Biol Chem.* 1999;274:12236–12244.
- [48] Cordin O, Beggs JD. RNA helicases in splicing. *RNA Biol.* 2013;10:83–95.
- [49] Ohmori H. Structural analysis of the rhlE gene of Escherichia coli. *Idengaku zasshi.* 1994;69:1–12.
- [50] Iost I, Dreyfus M. DEAD-box RNA helicases in Escherichia coli. *Nucleic Acids Res.* 2006;34:4189–4197.
- [51] Bernstein KA, Granneman S, Lee AV, et al. Comprehensive mutational analysis of yeast DEXD/H box RNA helicases involved in large ribosomal subunit biogenesis. *Mol Cell Biol.* 2006;26:1195–1208.
- [52] Nicol SM, Fuller-Pace FV. The “DEAD box” protein DbpA interacts specifically with the peptidyltransferase center in 23S rRNA. *Proc Natl Acad Sci U S A.* 1995;92:11681–11685.
- [53] Elles LM, Uhlenbeck OC. Mutation of the arginine finger in the active site of Escherichia coli DbpA abolishes ATPase and helicase activity and confers a dominant slow growth phenotype. *Nucleic Acids Res.* 2008;36:41–50.
- [54] Tan H, Zhang L, Weng Y, et al. PA3297 counteracts antimicrobial effects of azithromycin in pseudomonas aeruginosa. *Front Microbiol.* 2016;7:317.
- [55] Jagessar KL, Jain C. Functional and molecular analysis of Escherichia coli strains lacking multiple DEAD-box helicases. *Rna.* 2010;16:1386–1392.
- [56] Lehnik-Habrink M, Rempeters L, Kovacs AT, et al. DEAD-Box RNA helicases in Bacillus subtilis have multiple functions and act independently from each other. *J Bacteriol.* 2013;195:534–544.
- [57] Netterling S, Bareclav C, Vaitkevicius K, et al. RNA helicase important for listeria monocytogenes hemolytic activity and virulence factor expression. *Infect Immun.* 2016;84:67–76.
- [58] Sambrook J, Fritsch EF, Maniatis T. Molecular cloning: a laboratory manual. 2nd ed. Cold Spring Harbor (NY): Cold Spring Harbor Laboratory Press; 1989.
- [59] Ye RW, Haas D, Ka JO, et al. Anaerobic activation of the entire denitrification pathway in Pseudomonas aeruginosa requires Anr, an analog of Fnr. *J Bacteriol.* 1995;177:3606–3609.
- [60] Valentini M, Laventie BJ, Moscoso J, et al. The diguanylate cyclase HsbD intersects with the HptB regulatory cascade to control pseudomonas aeruginosa biofilm and motility. *PLoS Genet.* 2016;12:e1006354.
- [61] McCarthy RR, Valentini M, Filloux A. Contribution of cyclic di-GMP in the control of Type III and Type VI Secretion in Pseudomonas aeruginosa. *Methods Mol Biol.* 2017;1657:213–224.
- [62] Soding J, Biegert A, Lupas AN. The HHpred interactive server for protein homology detection and structure prediction. *Nucleic Acids Res.* 2005;33:W244–248.